Available online at www.sciencedirect.com
SCIENCE DIRECT®
Materials Science and Engineering C 26 (2006) 1202 – 1206
MATERIALS SCIENCE & ENGINEERING C
www.elsevier.com/locate/msec

Transmission electron microscopy study of carbon nanophases produced by ion beam implantation

I. Djerdj [a,*], A.M. Tonejc [a], M. Bijelić [a], M. Buljan [b], U.V. Desnica [b], R. Kalish [c]

[a] Department of Physics, Faculty of Science, Bijenicka cesta 32, PO Box 331, 10002 Zagreb, Croatia
[b] Rudjer Bošković Institute, PO Box 180 Zagreb, Croatia
[c] Physics Department and Solid State Institute, Technion, Haifa, Israel

Available online 12 October 2005

Abstract

The formation of carbon nanocrystals, produced by ion implantation of carbon ions into fused SiO_2 substrates, followed by 1 h thermal annealing at 1000 °C, in an Ar+5% H atmosphere has been studied. Combined high-resolution transmission electron microscopy (HRTEM) and selected area electron diffraction (SAED) have been employed for structural characterization of carbon nanophases embedded in the quartz substrate. The dependence of grain size and sample morphology of the carbon nanophases on implantation dose was studied. The carbon nanocrystals formed by the implantation for a dose of 1×10^{16} C/cm^2 at 320 keV have been identified as a mixture of *c*-diamond nanophase and a modified diamond nanophase known as *n*-diamond. For a higher implantation dose, 5×10^{16} C/cm^2, besides *n*-diamond, another solid carbon nanophase was observed, with a structure known as *i*-carbon. Following the highest implantation dose 1×10^{17} C/cm^2 the sample contained the *i*-carbon nanophase only. A least-square refinement of SAED patterns was employed for the calculation of unit-cell parameters of identified carbon nanophases.

Keywords: Transmission electron microscopy; Nanocrystalline diamond; Ion implantation; Electron emitter

1. Introduction

Different nanocrystalline (NC) materials, such as isolated nanoparticles supported on carriers or embedded in solid matrices, have attracted much attention due to their wide application. It was observed that the physical properties of such NC materials like melting point, phase transition temperature or hardness depend on grain size [1]. The variation in band gap with grain size allows for the tuning of luminescence wavelengths according to the aimed application [2]. Also, the large nonlinear properties of these materials make them applicable in waveguides, optical switches and bistable resonators [3]. One of the most versatile methods for fabricating nanocrystals is high-dose ion implantation. The versatility of this method is the consequence of the injection possibility of any impurity in any host matrix up to any desirable concentration [4]. The main disadvantage of this method is the damage inflicted onto the lattice by the implantation. If the implanted material is insoluble in the matrix, then annealing causes the formation of clusters and partially repairs the host lattice too. The implantation energy controls the depth, measured from the surface at which the ions are embedded; the implantation dose and energy determine the local concentration of the implants. These together with the annealing time determine the final size of nanocrystals.

The particular interest for synthesis of nanocrystalline carbon structures is the fact that carbon can bond in sp^1 (linear polymer-like), sp^2 (trigonal planar graphite-like) and sp^3 (tetrahedral diamond-like) hybridizations. The existence of three distinct nanocrystalline carbon phases has been previously reported [2,5–7]. Besides the cubic diamond (*c*-diamond) phase with the space group $Fd3m$, and unit cell parameter $a_0 = 0.356$ nm, other carbon nanophases can also be found following C ion-implantation and annealing. These include a metastable form of diamond known as a *n*-diamond (or γ-carbon) with *fcc* unit cell ($a_0 = 0.356$ nm) and a space group $Fm3m$, and a form of nanocrystalline carbon phase referred to as *i*-carbon in the literature [8] with the primitive

* Corresponding author. Tel.: +385 1 4605530; fax: +385 1 4680336.
E-mail address: idjerdj@phy.hr (I. Djerdj).

0928-4931/$ - see front matter © 2005 Elsevier B.V. All rights reserved.
doi:10.1016/j.msec.2005.09.015

cubic unit cell (a_0=0.432 nm) belonging to the space group $P2_13$ or $P4_232$.

Under atmospheric pressure and equilibrium conditions synthesis of *c*-diamond directly from the carbon atoms embedded in a solid matrix is not straightforward. Nanocrystalline *c*-diamond can be produced by a variety of methods including thin film deposition, detonation synthesis and shock explosion [5]. The potential application of nanocrystalline diamond is as a high-efficiency electron emitter for flat-panel displays. The recent success in synthesis of diamond nanocrystals was reported by Melbourne group and published in several articles [2,6,9]. They introduced carbon atoms into a fused-silica substrate by means of 1 MeV ion implantation to doses of 5×10^{16}, 2×10^{17} and 5×10^{17} C/cm^2 followed by 1 h thermal annealing at 1100 °C in forming gas (96% Ar + 4% H). It has resulted in the formation of cubic diamond nanocrystals embedded in the quartz matrix. It was also shown by Prawer and co-workers [9] that the formation of *c*-diamond phase was possible only within a very narrow range of implantation doses and annealing parameters; only the lowest dose, followed by annealing resulted in diamond formation. Higher doses and longer annealing times resulted in *n*-diamond, *i*-carbon or graphite formation. Annealing without the presence of hydrogen resulted in the diffusion of all implanted material out of the sample.

In this work, carbon ions were implanted into SiO_2 at different doses. Following annealing the samples were structurally characterized with the aid of the 200 kV high-resolution transmission electron microscopy (HRTEM) and selected-area electron diffraction (SAED). The aim of the present work was to investigate the phase composition, crystallographic parameters, morphology, average grain size and grain size distribution as a function of preparation conditions, i.e. implantation dose.

2. Experimental

Carbon ions were implanted into fused quartz substrate with an energy 320 keV at room temperature. Three doses of carbon ions were implanted: $D_1=1\times10^{16}$, $D_2=5\times10^{16}$ and $D_3=1\times10^{17}$ C/cm^2. Projected range was 800 nm with a straggling of 120 nm according to TRIM calculation [10]. Average concentrations near the maxima for three implanted doses are as follows: 3.3×10^{20} C/cm^3 for D_1, 1.6×10^{21} C/cm^3 for D_2 and 3.3×10^{21} C/cm^3 for the sample D_3. A quartz substrate was implanted with argon ions and served as a control sample. Implanted samples were annealed by furnace annealing (FA) processes at temperatures of 1000 °C for 1 h in forming gas (95% Ar + 5% H) environment. Heating rate was 6000 °C/h.

For TEM investigation the samples were prepared as follows: the implanted surface of the quartz glass plate was carefully abraded by a fine abrasive paper. The abraded particles were dispersed in ethanol and ground in ultrasonic bath. Finally, the particles were carefully set on a support copper grid coated with an amorphous carbon film. JEOL JEM-2010 200 kV microscope with a beryllium window energy-dispersive (EDS) detector was used for HRTEM and SAED investigations (Cs = 0.5 mm, point resolution 0.19 nm).

3. Results and discussion

Three samples with different implanted to C doses of: $D_1=1\times10^{16}$, $D_2=5\times10^{16}$, $D_3=1\times10^{17}$ C/cm^2 were examined. The results are presented in Table 1 and in Figs. 1–4. TEM image of sample D_1 was recorded at intermediate magnification and shown in Fig. 1(a) on which we can see that the material consists of quasi-isolated grains embedded in an amorphous matrix. The grains are of different shapes; some of them are quasi-spherical of different diameters, but there

Table 1
Results of the analysis of SAED patterns shown in Fig. 3(a)–(f)

	c-diamond	(a)	(b)	(c)	(d)	(e)	(f)	*n*-diamond	*i*-carbon	
hkl	*Fd3m* (a_0=0.356 nm) *d* (nm)	1×10^{16} C/cm^2 *d* (nm)	1×10^{16} C/cm^2 *d* (nm)	5×10^{16} C/cm^2 *d* (nm)	5×10^{16} C/cm^2 *d* (nm)	1×10^{17} C/cm^2 *d* (nm)	1×10^{17} C/cm^2 *d* (nm)	(a_0=0.356 nm) *d* (nm)	(a_0=0.432 nm) *d* (nm)	*hkl*
					0.2918				0.303	110
110^f	0.2517				0.2423		0.2423		0.249	111
111	0.2050	0.2072	0.2057	0.2087	0.2087	0.2057	0.2057	0.206	0.213	200
200^f	0.1780	0.1713	0.1744	0.1776	0.1821	0.1776		0.178	0.178	211
112^f	0.1453				0.1466	0.1466	0.1474		0.159	220
220	0.1258	0.1254	0.1260	0.1260	0.1271	0.1271	0.1243	0.126	0.129	311
311	0.1073	0.1063	0.1055	0.1108	0.1075	0.1075		0.107	0.109	400
222^f	0.1025					0.1029		0.104	0.105	410
004	0.0890							0.0898	0.0916	422
133	0.0816	0.0809	0.0806	0.0805				0.0818	0.0847	431
420^f	0.0796							0.0796		
224	0.0726							0.0726		
Refined value of unit-cell parameter a_0 (nm)		0.353(3)	0.354(7)	0.35(1)	0.40(1)	0.421(4)	0.42(1)			
Identified phases		*c* + *n*	*c* + *n*	*n*	*i*	*i*	*i*			
Average grain size *D* (nm)		(16.3 ± 1.1)	(15.8 ± 0.9)	(7.7 ± 0.3)	(6.9 ± 0.3)	(8.2 ± 0.3)	(7.4 ± 0.3)			

In addition, the *d*-spacings and belonging (*hkl*) reflections of three nanocrystalline carbon phases are also displayed. The superscript *f* corresponds to "forbidden" reflections of *Fd3m* diamond. The extracted values of unit cell parameters a_0 as well as identified phases (*c*-diamond (*c*), *n*-diamond (*n*), *i*-carbon (*i*)) are also displayed.

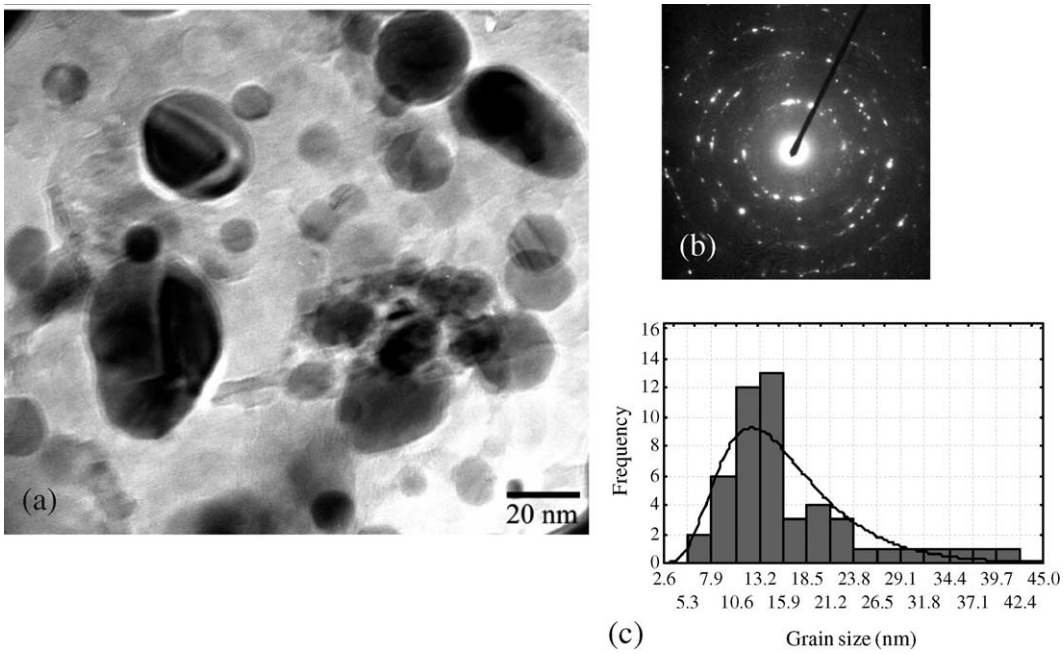

Fig. 1. (a) TEM image of 1×10^{16} C/cm^2 sample (D_1) showing diffraction contrast effects, implying triangular facets of diamond grains. (b) Corresponding SAED pattern with *c*-diamond and *n*-diamond identified phases. (c) The grain size distribution obtained from (a) and fitted to lognormal function.

exist also irregular grains with polyhedral facets. The facetting of the grains embedded into amorphous host is probably determined by minimization of the free energy of the entire system (crystallite+matrix) as suggested by Sutton and Balluffi [11].

The analysis of SAED pattern displayed in Fig. 1(b) is shown in Table 1 under the column marked (a) along with the data for *c*-diamond, *n*-diamond, and *i*-carbon, for comparison. The *hkl* reflections marked with superscript *f* in the column for *c*-diamond correspond to "forbidden" diffraction rings in *c*-diamond. It was evidenced that identified reflections of SAED pattern of D_1 fit well with diffraction lines of *c*-diamond. However, the presence of weak diffraction spots which correspond to (200) "forbidden" reflection of *c*-diamond indicates the presence of another phase. According to Refs. [2,6,9,12], the structure which also includes forbidden reflection (200), with *fcc* crystal structure was identified as a *n*-diamond. Therefore, according to Fig. 1(b), the sample D_1 consists of *c*-diamond as a dominant phase with a small amount of the *n*-diamond phase. Additional analysis of SAED

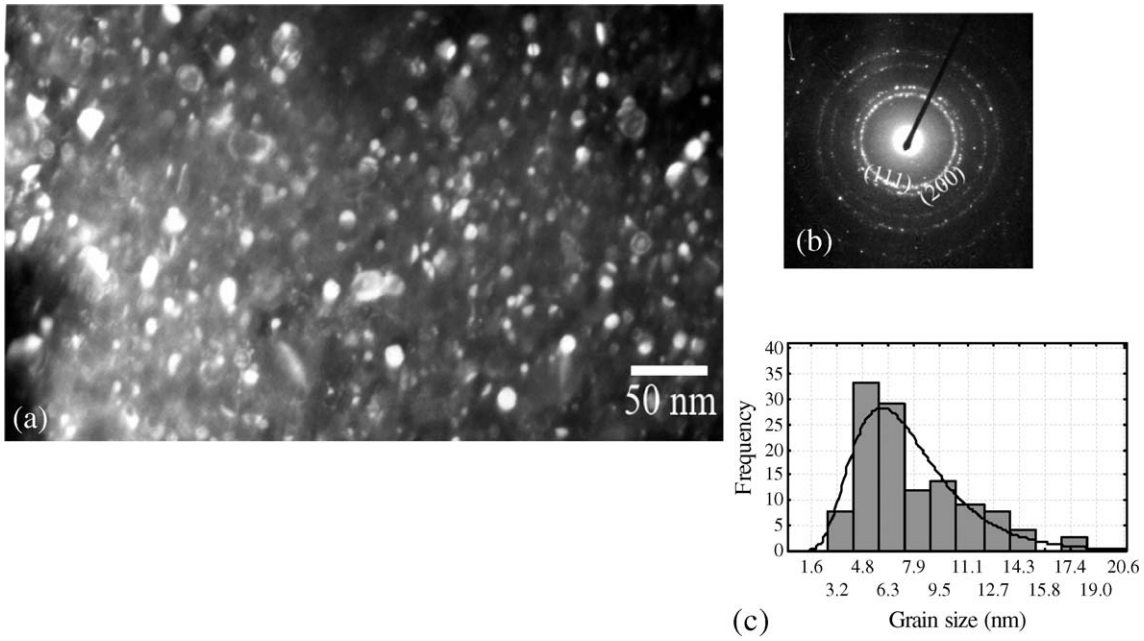

Fig. 2. (a) DF image of 5×10^{16} C/cm^2 sample (D_2) obtained from the part of (111) ring of *n*-diamond phase. (b) Corresponding SAED pattern with *n*-diamond identified phase. (c) The grain size distribution obtained from (a) and fitted to lognormal function.

pattern recorded at different position within the same sample has confirmed this finding. It is shown in Fig. 3(b), while the measured *d*-spacings and identified *hkl* reflections are also displayed in Table 1 (column (b)).

Cubic diamond grains with {111} facetting are the dominant growth form at low carbon implantation dose, showing well-defined triangle shape. Those facets are evidenced as the diffraction-contrast effects in Fig. 1(a). Considering grain sizes, it is evident that the investigated part of the sample is rather heterogeneous, i.e. yielding rather broad grain size distribution as shown in Fig. 1(c). The grain sizes are in the range between 6 nm and 40 nm, with the average value of (16.3±1.1) nm. However, the distribution maximum lies between 13.2 and 15.9 nm, and there is also a long distribution "tail" showing the existence of some large grains. The best fit of the empirical distribution is achieved by lognormal function, denoted by the solid line in Fig. 1(c).

Similar structural analysis was then performed on sample D_2. In Fig. 2(a), dark-field (DF) image is shown, while the corresponding SAED pattern is displayed in Fig. 2(b). The analysis of this SAED pattern is shown in Table 1 under the column marked (c). Since the intensity of the strongest

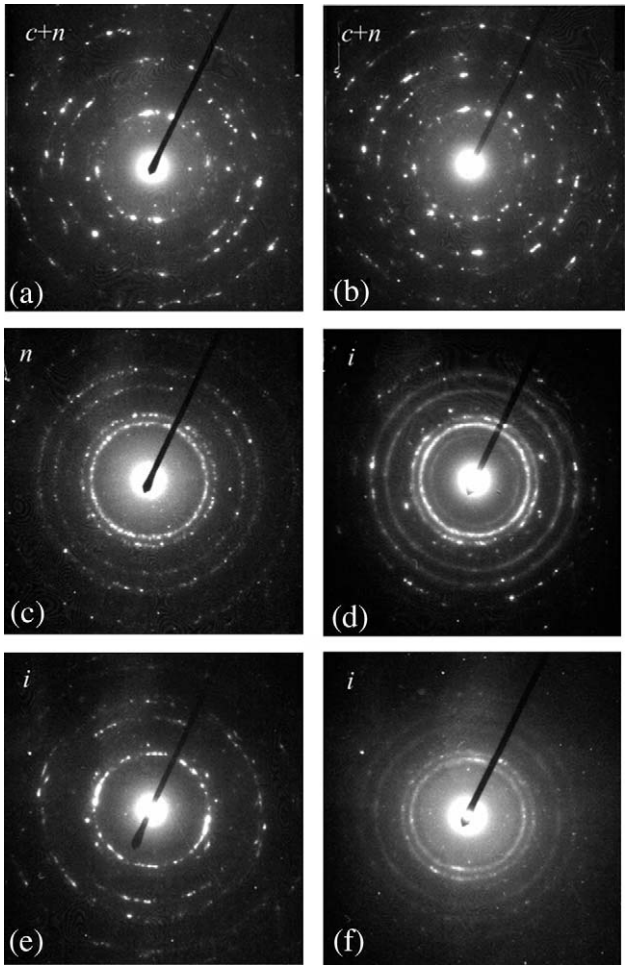

Fig. 3. SAED patterns of examined samples showing the sequence of nanocrystalline carbon phases as the ion dose increases: (a)–(b) 1×10^{16} C/cm^2 dose. (c)–(d) 5×10^{16} C/cm^2 dose. (e)–(f) 1×10^{17} C/cm^2 dose. Identified phases are marked with the letters: *c*-diamond (*c*), *n*-diamond (*n*), *i*-carbon (*i*).

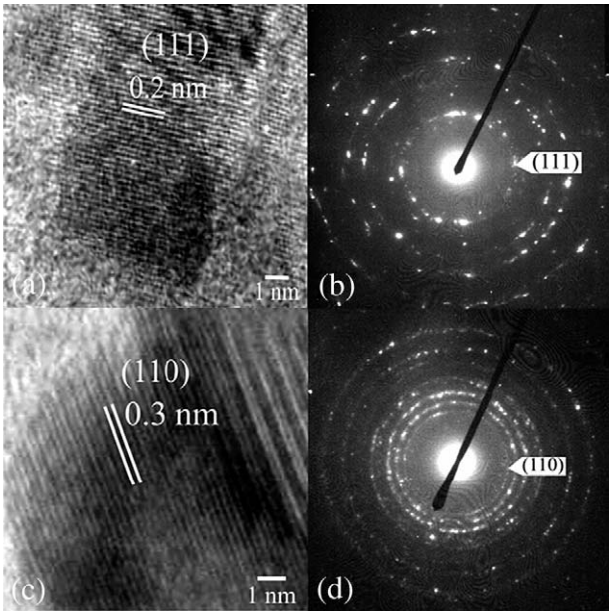

Fig. 4. (a) Enlarged HRTEM image of 1×10^{16} C/cm^2 sample (D_1) showing (111) lattice planes of *c*-diamond. (b) Corresponding SAED pattern with marked (111) reflection. (c) Enlarged HRTEM image of 5×10^{16} C/cm^2 sample (D_2) showing (110) lattice planes of *i*-carbon. (d) Corresponding SAED pattern with marked (110) reflection.

c-diamond reflection ring (111) is comparable with the intensity of "forbidden" reflection ring (200), the whole SAED pattern can be identified as *n*-diamond diffraction pattern. Another SAED pattern taken again at the different position within the sample D_2 is shown in Fig. 3(d). This pattern has more rings in comparison with Fig. 3(c) (or Fig. 2(b)), and indexed *d*-values are given in Table 1 under column (d). All those reflections can be well assigned to the *i*-carbon nanophase. Such observed feature, having different structure at different positions within the same sample, D_2 is an evidence of heterogeneity of investigated material.

The DF image is taken from the part of the brightest Debye–Scherrer ring of *n*-diamond phase (111) from corresponding SAED pattern. In comparison with the sample D_1, sample D_2 is more homogeneous in respect to the grain sizes and shape. The grain size range is between 4 and 18 nm, which is narrower in comparison with sample D_1; the average grain size is (7.7±0.3) nm, which is almost the half value of low dose sample D_1, and the distribution maximum lies in interval between 4.8 and 6.3 nm. The grains are of quasi-spherical shape and the grain size distribution is also best fitted against to lognormal function.

The analysis of the highest dose sample D_3 yields the average grain size of (8.2±0.3) nm. The SAED patterns of sample D_3 are shown in Fig. 3(e)–(f). According to them the indexing and *d*-spacings summarized in Table 1 under the columns (e) and (f) have shown that the reflection rings are consistent with *i*-carbon.

Using the formula for cubic crystal system, with the help of least-square refinement of SAED data, the values of unit cell parameters of carbon nanophases are extracted and given also in Table 1. There is a good agreement between our results and

previous reports [2,6,9] in unit cell parameter values of *c*-diamond, *n*-diamond, and *i*-carbon.

Fig. 4(a) shows HRTEM image of the crystal lattice of the *c*-diamond captured on sample D_1. The measured *d*-value of the lattice fringes is found to be 0.2 nm, which can be indexed as (111) reflection of *c*-diamond found and denoted also in corresponding SAED pattern (Fig. 4(b)). HRTEM image of *i*-carbon modification captured on sample D_2 is shown in Fig. 4(c). The lattice fringes with interplanar spacing of 0.3 nm, indexed as (110) reflection of *i*-carbon are clearly resolved. The same diffraction ring is intelligibly visible in corresponding SAED pattern displayed in Fig. 4(d). In both HRTEM 4(a) and 4(c) images Moiré fringes are observed as a result of the interference effect of different carbon nanophases with close values of *d*-spacing. In Fig. 4(c) it is visible that Moiré fringes are parallel with (110) lattice planes of *i*-carbon. This implies that the second nanophase which contributes to the Moiré fringe has also parallel reflecting planes. Using the analogue of two line gratings (carbon nanophases) a structure of larger periodicity is produced. Beats (Moiré fringes) are then formed between these two periodicities with spacing *D* given by $D = d_1 d_2/(d_1 - d_2)$, where d_1 and d_2 are the spacing of each grating. Measuring of the Moiré fringes periodicity in Fig. 4(c) yielded $D = 0.77$ nm, and considering d_1 being 0.3 nm, the calculated value of d_2 was 0.21 nm. According to the comprehensive SAED analysis of sample D_2, the reflecting planes with the spacing 0.21 nm were identified as (111) lattice planes of *n*-diamond. Therefore, the observed Moiré fringes in Fig. 4(c) served as an evidence of the simultaneous presence of *n*-diamond and *i*-carbon nanophases within the sample D_2.

We observed different carbon nanophase sequence with implantation dose increase in comparison with the results reported in Ref. [9]. Moreover, no pure nanocrystalline *c*-diamond phase was observed. This can be mainly attributed to the lower implantation energy (320 keV in comparison with 1 MeV) and partially to the different annealing conditions. We performed annealing at the temperature of 1000 °C which was lower in comparison with [9] (1100 °C) in the forming gas which contained 1% of hydrogen more than forming gas employed in [9]. The formation of clusters with particular phase is in sensitive dependence to the dose of the implanted carbon ions and to the depth of implanted carbon atoms (energy of the implantation). *C*-diamond nanophase is forming when the condition of low carbon concentration in near surface region is fulfilled. These can be controlled by low dose of implanted material and with deeper implantation of carbon ions [13]. In our experiment the implantation depth of carbon ions was 800 nm, which was considerably lower in comparison with [9] (1450 nm). Therefore, we believe that the main cause of the lack of pure *c*-diamond nanophase is low implantation energy employed in this work.

4. Conclusion

TEM and SAED study of carbon nanophases produced by ion beam implantation of 320 keV carbon ions to doses of 1×10^{16}, 5×10^{16}, 1×10^{17} C/cm^2 into fused SiO_2 substrates, followed by thermal annealing at 1000 °C in forming gas have revealed the following:

(i) The carbon clusters formed are nanocrystalline. The sample of the lowest dose has had almost spherical grains, whereas the presence of diffraction-contrast effects revealed triangle facetting of *c*-diamond nanophase. The medium and highest dose samples have rather spherical grains.

(ii) The phase composition sequence with implantation dose is as follows: 1×10^{16} C/cm^2 sample contains *c*-diamond as a major nanophase with *n*-diamond as a minor nanophase; 5×10^{16} C/cm^2 sample comprises *n*-diamond and *i*-carbon nanophases, while 1×10^{17} C/cm^2 sample is composed of *i*-carbon nanophase only.

(iii) HRTEM analysis has revealed resolved (111) lattice planes of *c*-diamond and (110) lattice planes of *i*-carbon. The analysis of the observed Moiré fringes has evidenced the simultaneous presence of *n*-diamond and *i*-carbon nanophases within the sample D_2.

Acknowledgement

We thank the Croatian Ministry of Science and Technology (Project Nos. 0119252, and 0098020) for financially supporting this work. The authors express their appreciation to Dr. C. Saguy and Dr. V. Richter, for helpful discussions and samples preparation.

References

[1] X. Ma, W. Shi, Mic. Eng. 66 (2003) 153.
[2] J.O. Orwa, S. Prawer, D.N. Jamieson, J.L. Peng, J.C. McCallum, K.W. Nugent, Y.J. Li, L.A. Bursill, J. Appl. Phys. 90 (6) (2001) 3007.
[3] M. Ivanda, K. Babocsi, C. Dem, M. Schmitt, M. Montagna, W. Kiefer, Phys. Rev., B 67 (2003) 5329.
[4] C.W. White, J.D. Budai, S.P. Withrow, J.G. Zhu, E. Sonder, R.A. Zuhr, A. Meldrum, D.M. Hembree Jr., D.O. Henderson, S. Prawer, Nucl. Instrum. Methods Phys. Res., B Beam Interact. Mater. Atoms 141 (1998) 228.
[5] S. Prawer, K.W. Nugent, D.N. Jamieson, J.O. Orwa, L.A. Bursill, J.L. Peng, Chem. Phys. Lett. 332 (2000) 93.
[6] J.L. Peng, L.A. Bursill, B. Jiang, J.O. Orwa, S. Prawer, Philos. Mag. B, 81 (12) (2001) 2071.
[7] S. Endo, N. Idani, R. Oshima, K.J. Takano, M. Wakatsuki, Phys. Rev. B, 49 (1) (1994) 22.
[8] B.G. Burkhard, K. Dan, Y. Tanabe, A.K. Sawaoka, K. Yamada, J. Appl. Phys. 33 (1994) 5875.
[9] S. Prawer, J.L. Peng, J.O. Orwa, J.C. McCallum, D.N. Jamieson, L.A. Bursill, Phys. Rev., B 62 (24) (2000) R16360.
[10] J.F. Ziegler, J.P. Biersack, U. Littmak, The stopping Powers and Ranges of Ions in Matter, Pergamon, New York, 1985.
[11] A.P. Sutton, R.W. Balluffi, Interfaces in Crystalline Materials, Clarendon Press, Oxford, 1996, p. 58.
[12] I. Konyashin, A. Zern, J. Mayer, F. Aldinger, V. Babaev, V. Khvostov, M. Guseva, Diamond Relat. Mater. 10 (2001) 99.
[13] M. Buljan, et al., Phys. Rev., B, (submitted for publication).